

# Modeling of free growth of a crystal during the stage of development of the dendrite form

A. M. Ovrukskii

*Dnepropetrovsk State University*

(Submitted 20 June 1990; resubmitted 24 September 1990)

*Zh. Eksp. Teor. Fiz.* **99**, 250–259 (January 1991)

A description is given of a method for numerical solution of the problem of growth of a crystal with a complex surface profile. Mathematical solutions of this problem predict dendritic form of growth in the case of a particle which precipitates out of a liquid solution when the supersaturation of this solution is high. Cases of different degrees of anisotropy of the kinetic coefficient (which can assume different values) and of the surface tension are considered. The other problems addressed in the paper relate to the steady-state growth of the tip of a dendrite, the influence of the anisotropy of the kinetic coefficient and surface tension on the shape of the dendrite core near the tip, and the influence of small random changes in the local growth rate ("noise") on the evolution of the shape of a crystal as a whole.

## 1. INTRODUCTION

Dendritic growth is the most common form of free growth of crystals, particularly of metals and other substances with a low value of the melting entropy. The solutions of the diffusion problem of crystal growth admit the possibility of steady-state growth in the shape of a parabolic needle.<sup>1–3</sup> It was shown in Ref. 4 that in the case of a finite surface tension  $\alpha$  this needle shape is in conflict with the boundary conditions. Wave perturbations of the paraboloid shape and the appearance of side branches were investigated by Langer and Muller-Krumbhaar.<sup>5,6</sup> It was established in Refs. 7–11 that if the surface tension  $\alpha$  is finite but anisotropic, there are steady-state mathematical solutions of the problem of dendrite growth (with a constant form of the tip and a constant growth rate). Specific growth rates are also preferred if the kinetic coefficient  $\beta$ , representing the relationship between the growth rate and the local surface supersaturation, is anisotropic.<sup>12,13</sup>

There have been few experimental investigations of dendrite growth (see, for example, Refs. 14–16) the results of which could be used in a comparison with the theory. Therefore, there is much current interest in modeling of dendrite growth. Calculations reported in Refs. 17–21 showed that projections of an initial shape of a crystal are not stable but split during growth if the coefficients  $\alpha$  and  $\beta$  are isotropic. However, such initial projections are stable if the coefficients  $\alpha$  and  $\beta$  are anisotropic. The results obtained by modeling do not yet reflect the great variety of the experimentally observed forms of crystal growth. For example, anomalous dendrites with a periodically varying form of the tip are frequently observed. The consecutive crystal profiles found by calculation in Refs. 17, 18, and 21 do not agree with the experimental observations of the splitting of tips.<sup>16</sup>

In most published simulations of free growth of crystals the starting point is the Laplace equation rather than the diffusion equation. We shall attempt to provide a satisfactory description of real dendritic growth of crystals by direct modeling based on the exact solution of the diffusion problem and determination of the whole concentration field describing a growing crystal.

## 2. NUMERICAL CALCULATION METHOD

The description of the growth of a crystal from a liquid solution will be based on the mathematical solution of the diffusion equation

$$\frac{\partial C}{\partial t} = D \nabla^2 C \quad (1)$$

(where  $C$  is the concentration of the diffusant and  $D$  is its diffusion coefficient) subject to a boundary condition which allows for the mass balance at the boundary between the phases:

$$(C_c - C_s) V = D (\partial C / \partial n). \quad (2)$$

Here,  $V$  is the growth rate,  $C_c$  is the concentration inside the crystal,  $C_s$  is the concentration in the liquid near the surface of the crystal, and  $\partial C / \partial n$  is the concentration gradient along the normal to the surface.

The local growth rate depends on the local supersaturation, which is related to the surface curvature  $K$  at the point in question, which follows from the Gibbs–Thompson condition generalized by Herring<sup>22</sup> to the case of an anisotropic surface energy. Therefore, if we describe the growth rate by

$$V = \beta(\varphi) (\sigma_s - \Gamma(\varphi) K), \quad (3)$$

we have to allow also for the anisotropy of the kinetic coefficient  $\beta(\varphi)$  and of the surface tension  $\alpha(\varphi)$ . Here,  $\varphi$  is the angle representing the orientation of a part of the surface (relative to the direction corresponding to the surface energy maximum),

$$\Gamma(\varphi) = (\alpha + \partial^2 \alpha / \partial \varphi^2) \Omega / kT.$$

$\Omega$  is the volume of a molecule, and  $\sigma_s = (C_s - C_e) / C_e$  is the relative supersaturation at the selected point on the surface. In describing the anisotropy of the coefficients  $\alpha$  and  $\beta$ , we shall adopt the following expressions which are frequently employed in theoretical calculations:

$$\alpha = \alpha_0 (1 + \epsilon_1 \cos 4\varphi), \quad \beta = \beta_0 (1 + \epsilon_2 \cos 4\varphi).$$

Consequently, we have

$$\Gamma(\varphi) = \Gamma_0 (1 - 15\epsilon_1 \cos 4\varphi),$$

where  $\Gamma_0 = \alpha_0 \Omega / kT$  is the capillary length.

We shall adopt a superposition of grids of two types in calculation of the concentration field in different parts of this liquid solution (Fig. 1). In the region of the solution near one of the growing projections we shall use a grid based on radial rays, similar to that used by us in Refs. 23–25. We shall describe the rest of the liquid solution by a grid consisting of “vertical” lines, which are perpendicular to the polar axis of the first grid, and of lines intersecting them and varying in shape from the profile of the crystal surface to the profile of the boundary of a container of a cell where the growth takes place, as the distance from the crystal increases. Such grids were used by us in Ref. 26 to find the temperature fields in a growing single crystal and in a melt. The lines intersecting the “verticals,” like the similar lines in the radial part, are drawn at intervals that increase in accordance with an arithmetic progression as we move away from the boundary between the phases. The two grids are matched along the line  $ON$  (Fig. 1), which is the last vertical and the first radial ray in the polar grid.

It is also known<sup>27,28</sup> that the best method for numerical solution of the transport equations in the case of complex boundary surfaces involves the use of orthogonal grids matched to the surfaces so that certain nodal lines coincide with them. Methods for constructing such grids are known.<sup>27,28</sup> They require solution of a large number of algebraic equations. In the case of moving phase boundaries it is necessary to modify the grids after each calculation step in the time domain, but this requires considerable computer time. We used semiorthogonal grids. Since the locations of the nodes were limited to radial lines or verticals (Fig. 1), calculations of the node positions in each time layer were made using very simple expressions

$$r(m, n) = \rho(m) + (R(m) - \rho(m))n(n-1)/(N(N-1)),$$

$$Y(m, n) = YS(m) + (RY(m) - YS(m))n(n-1)/(N(N-1)),$$

where  $r(m, n)$  and  $Y(m, n)$  are the coordinates of nodes of the grid  $\rho(m)$ ,  $YS(m)$  are the coordinates of the nodes on the surface of the crystal,  $R(m)$  and  $RY(m)$  are the corresponding coordinates of the edge of the container (cell) where the growth took place, and  $N-1$  is the number of intervals into which the distance  $R(m) - \rho(m)$  or  $RY(m) - YS(m)$  is divided.

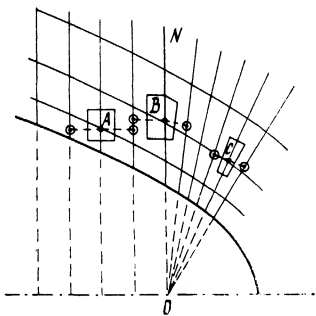


FIG. 1. Schematic representation of a calculation grid. Here,  $ON$  is the line of matching of grids of two types;  $A$ ,  $B$ , and  $C$  are calculation cells used in computation of concentrations at the network nodes.

The same precision of the calculations based on the diffusion equation was achieved for different grid because an increase in the concentration at given nodes during a short time interval  $\Delta t$  can be expressed in terms of the flux of matter along the boundaries of calculation cells of the type  $A$ ,  $B$ , and  $C$  shown in Fig. 1. Additional nodes (on the dashed lines) are shown near these calculation cells and at these nodes the concentration must be calculated first in order to determine the fluxes normal to the boundaries. Such orthogonal calculation cells can be used to fill the whole investigated region, so that the condition of conservation of the total amount of matter is obeyed. At the line matching the two grids a specific calculation cell  $B$  consists of two parts, one of which is rectangular and the other is radial. It follows from the calculations that the matching line does not perturb significantly the concentration field.

The constancy of the density of nodes on the surface of a crystal was ensured as follows: a periodic increase of the coordinate of a surface, linked to the polar axis, by a definite amount  $BX$  equal to the distance between the verticals was accompanied by transfer of the pole  $O$  of the radial grid (Fig. 1) by the same distance. Then, a new vertical  $ON$  and all the radial rays were drawn from there. In this way the whole grid and the number of the surface nodes increased with time. In our calculations the number of such surface nodes reached 55 or 95 for a  $90^\circ$  sector of a crystal.

### 3. RESULTS OF CALCULATIONS

Our calculations were carried out in the case of precipitation of a single-component crystal from a binary melt containing 80% of the substance to be precipitated. The diffusion coefficient  $D = 2.8 \times 10^{-5}$  cm<sup>2</sup>/s and the capillary length  $\Gamma_0 = 2.24 \times 10^{-8}$  cm corresponded to the precipitation of tin from a binary metallic melt (for example, Bi–Sn).

Figures 2a and 2b showed the mathematical solutions obtained for the isotropic coefficients  $\alpha$  and  $\beta$  ( $\beta = \beta_0 = 5$  cm/s) obtained for a circular container where the growth took place and a fairly strong supersaturation  $\sigma_\infty = (C_\infty - C_e)/C_e = 0.127$  ( $C_\infty = 0.8$  is the initial concentration of the liquid solution and  $C_e = 0.71$ ) assuming different degrees of distortion of the initial shape:  $\rho(\theta)/R^* = 300 + 19 \cos 4\theta$  for results in Fig. 2a and  $\rho(\theta)/R^* = 300 + 5 \cos 4\theta$  for Fig. 2b; here,  $\theta$  is the angle relative to the polar axis and  $R^* = \Gamma_0/\sigma_\infty$  is the radius of a critical nucleus. In the case of the adopted supersaturation the finite size of the growth container ( $6400R^*$ ) had no influence on crystal growth. During the investigated time the initial homogeneous supersaturated concentration field was retained far from the crystal. The initial concentration field near the crystal was specified in accordance with the results of the mathematical solution of the problem of growth of an isotropic particle in the size range from  $15R^*$  to  $300R^*$ .

Figure 3 shows the dependences of the radius of curvature  $\rho_t$  of the tip of a projection growing under surface supersaturation conditions and of the growth rate on the size of a crystal ( $R$  is the distance from the center of the crystal to the tip of the projection), which correspond to the mathematical solution shown in Fig. 2a. It is clear from Fig. 3 that the mathematical solutions obtained are unstable. The degree of surface supersaturation and the growth rate decrease monotonically. The radius of curvature of the tip of a growing

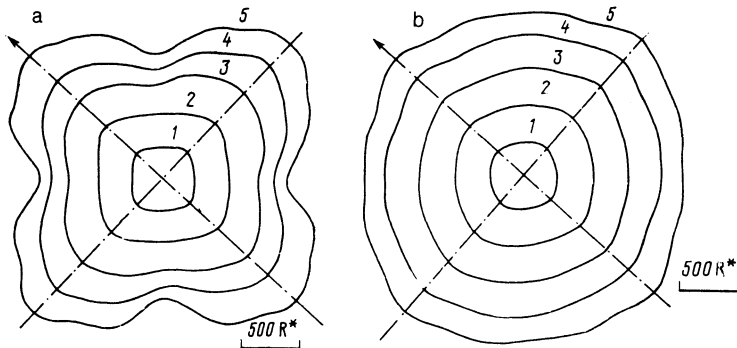


FIG. 2. Consecutive profiles of crystals growing in an axisymmetric container, calculated for the case when  $\sigma_\infty = (C_\infty - C_e)/C_e = 0.127$  ( $P = 0.055$ ),  $\varepsilon_1 = \varepsilon_2 = 0$ ,  $\beta_0 = 5$  cm/s. The profiles 1-5 are calculated for the following times: a) 0, 0.00089, 0.00194, 0.003, and 0.004 s; b) 0, 0.00091, 0.002, 0.0031, and 0.0042 s.

projection however remains constant in the range of sizes from  $1000R^*$  to  $1500R^*$ , although the average curvature of the region near the initial projection decreases. In the case of both initial forms of a crystal corresponding to the mathematical solutions shown in Figs. 2a and 2b the radii of curvature of the projection tips are approximately the same, but all the profiles in Fig. 2b are distorted as a whole (though relatively weakly). The subsequent profiles (also shown in Figs. 2a and 2b) are almost symmetric, although different grids were used by us for different regions of the diffusion zone. In the case of the weakly distorted form (Fig. 2b) the asymmetry is slightly less (down to 4% of the last profile). This case is characterized by a stronger mutual influence of the form and concentration profile, resulting in a higher growth rate of the more developed projection.

In contrast to the calculations valid in the range of low supersaturations,<sup>17,21</sup> based on the Laplace equation, in our case (Fig. 2) an increase in the size of a crystal results in preferential growth not of eight but of twelve projections. Then, stabilization of the values of the radius of curvature of the tips of the initial projections in the range of sizes from  $1000R^*$  to  $1500R^*$  is clearly related to the development of new bent parts of the surface, representing a new harmonic (namely the third characterized by  $k = 12$ ) of the wave-like distortion of the shape.

Figure 4 shows the dependences of the radius of curvature  $\rho_t$  of a growing tip on the values of the parameters  $\varepsilon_1$  and  $\varepsilon_2$ , which represent the anisotropy of the coefficients  $\alpha$

and  $\beta$  for the mathematical solutions obtained assuming the other parameters to be exactly the same as those used to obtain the results in Fig. 2a (crystal size  $1500R^*$ ). It is clear from Fig. 4 that the dependence of  $\rho_t$  on the values of the parameters  $\varepsilon_1$  and  $\varepsilon_2$  is monotonic. The dependence has no singularities in the limits  $\varepsilon_1 \rightarrow 0$  and  $\varepsilon_2 \rightarrow 0$ . For all the mathematical solutions obtained in the investigated range of sizes ( $1500R^*$ ) the rate of growth decreases monotonically.

The feasibility of steady-state growth when the concentration field is artificially kept in a steady state was tested by obtaining mathematical solutions for a lower degree of supersaturation ( $\sigma_\infty = 0.0666$ ) when the size of the growth container is increased along the polar axis. At the edge of this container in the "polar" region the supersaturation is assumed to have the initial value. Figure 5a demonstrates consecutive profiles of the crystal for this solution obtained subject to the isotropy of the coefficients  $\alpha$  and  $\beta$ . Figure 5b represents the solution for the anisotropic coefficient  $\alpha$ . In the case of the solution with the isotropic coefficients the radius of curvature of the projection tips increases slowly (Fig. 6) and its change in the range of sizes from  $1000R^*$  to  $2000R^*$  represents no more than 10% of the average value  $250R^*$ . The solution with the anisotropic surface tension (Fig. 5b,  $\varepsilon_1 = 0.04$ ) is nearly steady-state. In this case in the same range of sizes the deviations of the radius of curvature of the tip from the average value  $84R^*$  do not exceed 1% and changes in the rate of growth are also small (Fig. 6).

Several mathematical solutions were obtained for a high value of the kinetic coefficient  $\beta_0 = 250$  cm/s and they

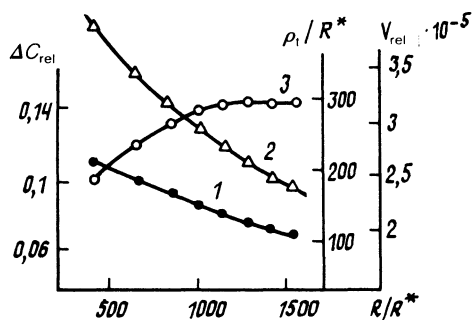


FIG. 3. Dependences of the relative value of the surface supersaturation  $\Delta C_{rel} = (C_t - C_e)/(C_\infty - C_e)$ , of the growth rate  $V_{rel} = V_t/R^*$ , and of the relative value of the radius of curvature  $\rho_t/R^*$  of the tip of a growing projection (curves 1, 2, and 3, respectively) on the size of a crystal (measured in terms of distances from the center of the crystal to the tip of a projection), plotted on the basis of the mathematical solution presented in Fig. 2a.

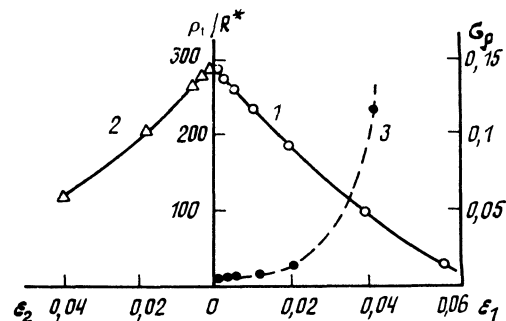


FIG. 4. Dependences of the relative value of the radius of curvature  $\rho_t/R^*$  of the tip of a projection (curves 1 and 2) and of the quantity  $\sigma_p = 2\Delta\Gamma/\rho_t^2 V$  (curve 3) on the values of the anisotropy parameters  $\varepsilon_1$  and  $\varepsilon_2$ ;  $\beta = \beta_0 = 5$  cm/s.

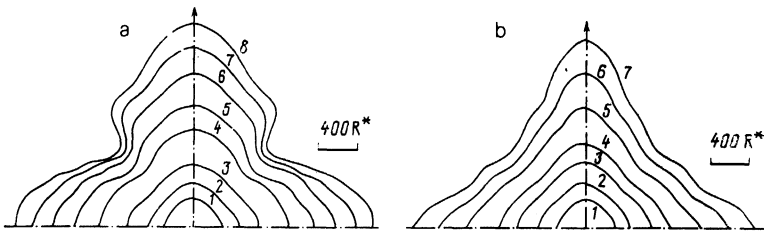


FIG. 5. Consecutive profiles of crystals in a container of increasing size, calculated for  $\beta = \beta_0 = 25$  cm/s,  $\sigma_\infty = 0.0666$  ( $P = 0.023$ ): a)  $\epsilon_1 = \epsilon_2 = 0$ , profiles 1–8 correspond to times  $t = 0, 0.0027, 0.0063, 0.01, 0.017, 0.025, 0.032$ , and  $0.039$  s; b)  $\epsilon_1 = 0.04, \epsilon_2 = 0$ , profiles 1–7 correspond to times  $t = 0, 0.0028, 0.0065, 0.01, 0.018, 0.026$ , and  $0.033$  s.

were characterized by random changes (“noise”) of the rate of motion of surface nodes, representing about 20% of the average value. Figures 7a and 7b showed two such mathematical solutions for the anisotropic coefficients  $\beta$  and  $\alpha$ , respectively. An increase in the crystal size results in this case in an initial development of 12 and then of 20–24 projections. The growth shape is highly unstable if the surface tension is anisotropic. Figure 7b shows periodic changes in the tip shape (corresponding to very large changes in the radius of curvature of the tip  $\rho_t$ ). On the whole, this pattern of evolution of the shape of the crystal resembles the growth of anomalous dendrites described in Ref. 15.

The tip shape predicted by the mathematical solutions obtained assuming that the coefficients  $\alpha$  and  $\beta$  are isotropic differs only slightly from the parabolic profile. For example, in a region of size  $2\rho_t$  adjoining a tip the profile 8 of Fig. 5a can be described satisfactorily by a parabola with a focal parameter  $p = 300R^*$ . The computer-calculated value of  $\rho_t$  for this profile is  $270R^*$ . The deviations of the tip profile from a parabola increase on increase in the parameters  $\epsilon_1$  and  $\epsilon_2$ , representing the anisotropy of the coefficients  $\alpha$  and  $\beta$ . For example, in the case of the profile 7 in Fig. 5b, we have  $\rho_t = 85$ , whereas a parabola approximating on the average satisfactorily this tip has a focal parameter  $p = 150R^*$  (for a perfect parabola it should be  $p = \rho_t$ ).

#### 4. DISCUSSION OF RESULTS

It follows from the calculations of Ref. 21 that in the case of a sufficiently large crystal which has specified initial distortions corresponding to one wave number  $k = 4$  (four projections) the growth is accompanied by the development of higher harmonics of the wave distortion of the shape (these are the second, third, and fourth harmonics characterized by  $k = 8, 12$ , and  $16$ ). Since in the case of the third and fourth harmonics the amplitudes of these distortions

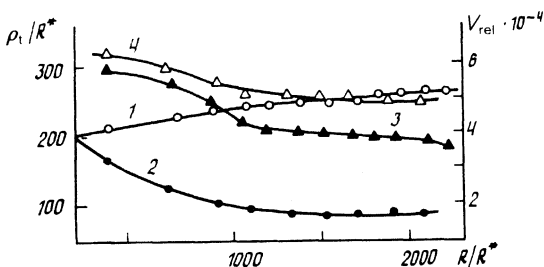


FIG. 6. Dependences of the relative growth rate  $V_{rel} = V/R^*$  (curves 3 and 4) and of the relative radius of curvature of the tip  $\rho_t/R^*$  (curves 1 and 2) of the main projections on the crystal size; curves 1 and 3 correspond to the profiles in Fig. 5a, whereas curves 2 and 4 correspond to the profiles in Fig. 5b.

grow slowly, in the range of sizes from  $1000R^*$  to  $2000R^*$  the splitting of the initial projections produces a shape with eight projections, corresponding to the strongest development of the second harmonic. In our calculations the shape with eight projections is intermediate and is obtained only for the mathematical solutions describing the case with a small initial distortion amplitude (Fig. 2b). The initial projections are then retained and there is no splitting. The reason for this is clearly the difference between the concentration fields obtained by solving the Laplace equation and those based on the diffusion equation. If a concentration field ensuring a better supply of matter to the projections is established in the course of growth, the “memory” of the initial concentration field may ensure that these projections are retained and grow preferentially during the subsequent stages.

In the two-dimensional case it is practically impossible to establish experimental conditions which would correspond to the mathematical solution of the Laplace equation. One would need to ensure very weak supersaturations in a very large container, because (in the view of the low growth rate) the region or the zone of the influence of a growing crystal as a result of diffusion becomes very large for a small increase in the size of the crystal. Photographs of ice crystals of individual projections undergoing splitting<sup>16</sup> suggest that random splitting is more likely. Such splitting is not related precisely to tips of the projections and after splitting the projection profiles are on the whole conserved, remaining similar to the profiles shown in Fig. 5a. However, according to the calculations of Refs. 17 and 21, the splitting of the initially present projections is a consequence of slow evolution of the whole profile of a crystal.

The dependences of the radii of curvature of tips of the projections on the parameters  $\epsilon_1$  and  $\epsilon_2$  (Fig. 4) have no singularities in the limits  $\epsilon_1 \rightarrow 0$  and  $\epsilon_2 \rightarrow 0$ , whereas according to Refs. 7–13 there are no steady-state mathematical solutions of the problem of growth by diffusion when the coefficients  $\alpha$  and  $\beta$  are isotropic. Our calculations allow us to follow the development of the profile of a growing crystal also when the coefficients  $\alpha$  and  $\beta$  are isotropic. The solutions presented in Figs. 2–4 are not in conflict with the theoretical predictions of Refs. 7–13 because they apply to the initial unsteady stage of growth. A recent paper<sup>29</sup> reported a rigorous calculation of the dependence of the criterion  $\sigma_\rho = 2D\Gamma/\rho_t^2V$ , which governs the selection rule applicable to the mathematical solutions with specific values of  $\rho_t$  and  $V$ , on  $\epsilon_1$ ; this dependence was obtained for two values (0 and 0.25) of a number  $P = \rho_t V/2D$ , which is a function of the supersaturation and governs the relationship between  $\rho_t$  and  $V$  when the growth shape is a paraboloid or a parabola.<sup>1,11</sup> It follows from this dependence that  $\sigma_\rho \rightarrow 0$  when  $\epsilon_1 \rightarrow 0$ . Consequently, if  $P$  is not equal to zero we find that

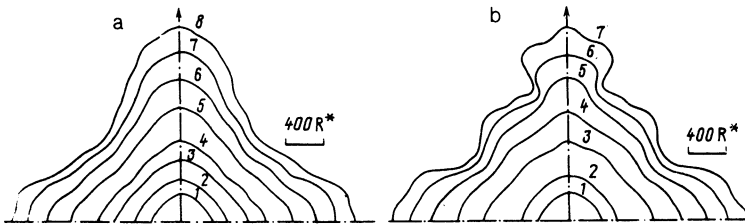


FIG. 7. Consecutive profiles of a crystal calculated for  $P = 0.023$  and  $\beta_0 = 250$  cm/s: a)  $\varepsilon_1 = 0$ ,  $\varepsilon_2 = 0.15$ , profiles 1–8 correspond to times  $t = 0, 0.0027, 0.0063, 0.01, 0.017, 0.025, 0.032$ , and  $0.039$  s; b)  $\varepsilon_1 = 0.01$ ,  $\varepsilon_2 = 0$ , profiles 1–7 correspond to times  $t = 0, 0.0027, 0.1, 0.17, 0.025, 0.032$ , and  $0.039$  s.

$\rho_t = \Gamma / (P\sigma_\rho) \rightarrow \infty$  in the limit  $\varepsilon_1 \rightarrow 0$ . In our solutions the tip radius  $\rho_t$  is finite not only for the unstable solutions (Figs. 2–4), but also for the solutions in which the concentration field approaches the steady-state form (Fig. 5).

The theoretical treatments reported in Refs. 7–13 deal with the growth forms or shapes differing from a parabolic needle only in the vicinity of the tip of a crystal. In fact, only very anisotropic crystals grow to form needles. If the anisotropy of the coefficients  $\alpha$  and  $\beta$  is low, branched or dendritic crystals are formed. The region adjoining the tip of a dendrite is subject to wave distortions of the shape and these are responsible for the appearance of the side branches.

The value  $\sigma_\rho = 0.025$  proposed in Ref. 6 was found assuming steady-state growth of a paraboloid with a periodically perturbed shape. Our mathematical solutions are in qualitative agreement with this earlier estimate ( $\sigma_\rho = 0.01$ – $0.014$  for the isotropic solutions characterized by different values of  $\beta$ ), although we are dealing with two-dimensional rather than three-dimensional growth. An increase in the degree of anisotropy increases  $\sigma_\rho$  (curve 3 in Fig. 4). In the case of the solutions shown in Fig. 5b, we have  $\sigma_\rho = 0.1$ , which is in agreement with the calculations reported in Ref. 29.

If the coefficient  $\alpha$  or  $\beta$  is strongly anisotropic, the region of wave distortions of the shape seems to move away from a tip (Fig. 5b) and there is an increase in the ratio of the wavelength ( $\lambda$ ) of distortion of the growth profile to the radius of curvature of the tip. Under these conditions it is physically meaningful to compare the results of calculations and the theory of growth of a parabolic needle. If the anisotropy of the coefficients  $\alpha$  and  $\beta$  is low or if there is no such anisotropy, the ratio  $\lambda / \rho_t$  is considerably less (Fig. 5a). Therefore, the mutual influence of the newly formed wave-like distortions of the surface profile near the tip and of the profile of the tip itself becomes important. Periodic appearance of new projections or inflections of the surface at a short distance from a tip may give rise to periodic changes in the tip curvature. An increase in the total number of projections in the profile of a crystal can be regarded also as the result of motion of a wave from regions where initially the parts of the surface lag behind (and the distortion amplitude is maximal) toward the tips of the projections. If such a wave catches up with a tip, the growth of the latter becomes unsteady.

Several mathematical solutions illustrate in Fig. 8 the changes which occur on increase in the quantity  $P_t = \rho_t V_t / 2D$ , representing the calculated values of the curvature of a tip and of the rate of its growth (i.e., the calculated values of the number  $P$ ). It is clear from this figure that the mathematical solution characterized by an anisotropic value of the coefficient  $\alpha$  (curve 2, corresponding to

$\beta = \beta_0 = 25$  cm/s) becomes practically steady on increase in the crystal size. On the other hand, the mathematical solution obtained for isotropic coefficients (curve 3) is oscillatory. Such oscillatory growth is unsteady (which is not in conflict with the theory), but the radius of curvature of the tip no longer becomes infinite. This radius is finite and it varies periodically. If such periodic variations are relatively slight, they may not be detected experimentally.

We can see from Fig. 8 that the mathematical solution with an anisotropic coefficient  $\beta$  (curve 4) and a high value of the “noise” of the local growth rate is also of unsteady oscillatory nature. In the case of an analogous mathematical solution shown in Fig. 7b (with an anisotropic coefficient  $\alpha$ ) the changes in the value of  $P_t$  are so large that they cannot be fitted into this figure. Such mathematical solutions are characterized also by a rapid growth of harmonics of wave perturbation of the form corresponding to a large number of projections. The development of higher-order harmonics is naturally associated with the “noise” level, since the rate of increase of their amplitude increases with the amplitude itself.<sup>24,30</sup> When the “noise” level is high, the starting values of the amplitudes of all the harmonics that can grow are also high.

In principle, noise is always present in numerical solutions. It follows from our solutions that the noise level influences the evolution of the shape of a crystal. However, in the mathematical solution for an infinitely large coefficient  $\beta$  but a low noise, when the surface concentration is in equilibrium for a given curvature of the surface and growth rates are found from the condition of balance of matter at the phase boundary, the accelerated growth of higher harmonics of distortion of the growth shape is no longer observed.

The question arises whether the noise associated with the effects of some real physical factors, such as fluctuations

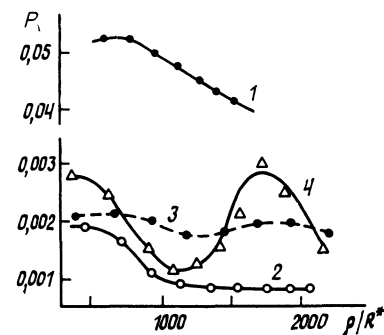


FIG. 8. Dependences of the values of the number  $P_t = \rho_t V_t / 2D$  on the size of crystals; the curves correspond to the following patterns: 1) Fig. 2a; 2) Fig. 5b; 3) Fig. 5a; 4) Fig. 7a.

of the temperature or contributions of transient convective fluxes on the transport of heat or matter, can influence the development of the shape of a crystal. It seems to us that such an influence does indeed exist. There is no other reasonable explanation of the formation of anomalous dendrites described in Ref. 15. However, in such cases the noise should be regarded as a real technological factor and a comprehensive analysis of its influence would be desirable.

The author regards it as his pleasant duty to thank E. A. Brener and O. P. Fedorov for discussing formulation of the problem.

- <sup>1</sup>G. P. Ivantsov, Dokl. Akad. Nauk SSSR **58**, 567 (1947).
- <sup>2</sup>M. E. Glicksman and R. J. Schaefer, J. Crystal Growth **2**, 239 (1968).
- <sup>3</sup>D. E. Temkin, Dokl. Akad. Nauk SSSR **132**, 1307 (1969).
- <sup>4</sup>G. F. Bolling and W. A. Tiller, J. Appl. Phys. **32**, 2587 (1961).
- <sup>5</sup>J. S. Langer and H. Muller-Krumbhaar, J. Crystal Growth **42**, 11 (1977).
- <sup>6</sup>J. S. Langer and H. Muller-Krumbhaar, Acta Metall. **26**, 1681 (1978).
- <sup>7</sup>M. Ben-Amar and Y. Pomeau, Europhys. Lett. **2**, 307 (1986).
- <sup>8</sup>D. A. Kessler, J. Koplik, and H. Levine, Phys. Rev. A **31**, 1712 (1985).
- <sup>9</sup>D. Kessler and H. Levine, Phys. Rev. B **33**, 7867 (1986).
- <sup>10</sup>A. Barbieri, D. C. Hong, and J. S. Langer, Phys. Rev. A **35**, 1802 (1987).
- <sup>11</sup>E. A. Brener, C. É. Esipov, and V. I. Mel'nikov, Zh. Eksp. Teor. Fiz. **94**(3), 236 (1988) [Sov. Phys. JETP **67**, 565 (1988)].
- <sup>12</sup>M.-A. Lemieux, J. Liu, and G. Kotliar, Phys. Rev. A **36**, 1849 (1987).
- <sup>13</sup>E. A. Brener, M. B. Geilikman, and D. M. Temkin, Zh. Eksp. Teor. Fiz. **94**(5), 241 (1988) [Sov. Phys. JETP **67**, 1002 (1988)].
- <sup>14</sup>S. C. Huang and M. E. Glicksman, Acta Metall. **29**, 701 (1981).
- <sup>15</sup>A. G. Borisov, V. V. Maslov, and O. P. Fedorov, Metallofizika **9**(6), 48 (1987).
- <sup>16</sup>S. H. Tirmizi and W. N. Gill, J. Crystal Growth **96**, 277 (1989).
- <sup>17</sup>D. Kessler, J. Koplik, and H. Levine, Phys. Rev. A **30**, 2820 (1984).
- <sup>18</sup>D. A. Kessler, J. Koplik, and H. Levine, Phys. Chem. Hydrodyn. **6**, 507 (1985).
- <sup>19</sup>Y. Saito, G. Goldbeck-Wood, and H. Muller-Krumbhaar, Phys. Rev. Lett. **58**, 1541 (1987).
- <sup>20</sup>D. I. Meiron, Phys. Rev. A **33**, 2704 (1986).
- <sup>21</sup>L. N. Brush and R. F. Sekerka, J. Crystal Growth **96**, 419 (1989).
- <sup>22</sup>C. Herring, in *Structure and Properties of Solid Surfaces (Proc. Conf., Lake Geneva, WI, 1952*, ed. by G. Gomer and C. S. Smith), University of Chicago Press (1953), p. 5.
- <sup>23</sup>A. M. Ovrutskii, Kristallografiya **23**, 925 (1978) [Sov. Phys. Crystallogr. **23**, 522 (1978)].
- <sup>24</sup>A. M. Ovrutskii, Kristallografiya **24**, 571 (1979) [Sov. Phys. Crystallogr. **24**, 327 (1979)].
- <sup>25</sup>A. M. Ovrutskii, Izv. Akad. Nauk SSSR Met. No. 4, 80 (1980).
- <sup>26</sup>A. M. Ovrutskii and I. V. Spiridonova, *Modeling of Crystallization Processes* [in Russian], The Dnepropetrovsk State University (1985).
- <sup>27</sup>J. F. Thompson, Z. U. A. Warsi, and C. W. Mastin, J. Comput. Phys. **47**, 1 (1982).
- <sup>28</sup>J. F. Thompson (ed.), *Numerical Grid Generation*, North-Holland, Amsterdam (1982).
- <sup>29</sup>A. Barbieri and J. S. Langer, Phys. Rev. A **39**, 5314 (1989).
- <sup>30</sup>L. N. Brush, R. F. Sekerka, G. B. McFadden, J. Crystal Growth **100**, 89 (1990).

Translated by A. Tybulewicz